ADVANCED MATERIALS
www.advmat.de

www.MaterialsViews.com

Orientationally Ordered Colloidal Co-Dispersions of Gold Nanorods and Cellulose Nanocrystals

*Qingkun Liu, Michael G. Campbell, Julian S. Evans, and Ivan I. Smalyukh**

Self-assembly of mesoscale structures composed of nano-sized functional units such as quantum dots and plasmonic metal nanoparticles is an exceptionally promising way of designing artificial composite materials with new macroscopic physical behavior and properties.[1–3] Self-assembly of anisotropic nanoparticles dispersed in responsive liquid crystalline host media may enable new composites with properties controlled by applying fields, changing temperature, and using other external stimuli.[4–10] Different approaches have been recently used for assembling nanoparticles, such as DNA conjugation,[1] polymer matrix engineering,[11] templating,[12] liquid crystal dispersion,[13–15] etc. However, stable and scalable organization of nanoparticles still remains a challenge, especially in terms of fabricating nano-structured materials with surface plasmon resonance (SPR) properties from renewable, biocompatible sources. Cellulose, which can be easily derived from cotton, wood and bacteria, is the most abundant renewable biopolymer available.[16] When cellulose fibers are subjected to acid hydrolysis, the fibers yield mono-domain, rod-like crystalline residues, dubbed "cellulose nanocrystals" (CNCs), which can self-organize into nematic and cholesteric lyotropic LC phases.[16] One of the most striking properties of CNCs is that the nematic or cholesteric order can be preserved after complete water evaporation,[17] providing a robust matrix for assembling nanoparticles compared with their surfactant-based lyotropic[15] or thermotropic liquid crystalline counterparts.[14] Although CNCs have been extensively studied from the standpoints of view of their morphology, chemistry and self-assembly, their potential applications in fabrication of nanocomposites and interaction with other nanoparticles remain relatively unexplored.

Dr. Q. Liu, M. G. Campbell, Dr. J. S. Evans,
Prof. I. I. Smalyukh
Department of Physics
University of Colorado
Boulder, CO, 80309, USA
E-mail: ivan.smalyukh@colorado.edu
Prof. I. I. Smalyukh
Department of Electrical
Computer, and Energy Engineering
Materials Science and Engineering Program
and Liquid Crystal Materials Research Center
University of Colorado
Boulder, CO, 80309, USA
Prof. I. I. Smalyukh
Renewable and Sustainable Energy Institute
National Renewable Energy Laboratory and University of Colorado
Boulder, CO, 80309, USA

DOI: 10.1002/adma.201402699

In this work, we develop cellulose-based orientationally ordered soft matter composites with polarization-dependent properties. In particular, we describe the use of colloidal dispersions of CNCs in mesomorphic phases as host materials capable of aligning gold nanorods (GNRs) with much smaller aspect ratios. When the concentration of electrostatically charged CNCs exceeds a certain critical concentration, the CNC dispersion transitions from an isotropic phase to a nematic-like order.[18] Entropic/excluded-volume effects prompt the GNRs to orient along the CNCs in mesomorphic phases of dispersions, with the strength of this alignment growing with increasing the CNC concentration. Therefore, we observe a transition from an initial orientationally disordered dispersion of GNRs to that with a uniaxial order mimicking that of CNCs and exhibiting polarization-dependent plasmonic extinction. Polarized optical microscopy (POM), micro-spectroscopy, two-photon luminescence (TPL) microscopy and transmission electron microscopy (TEM) are utilized to study the nematic-like and helicoidal structures of GNRs in CNCs co-dispersions. Additionally, we observe helicoidal configurations and cholesteric-isotropic biphasic coexistence of GNR-CNC co-dispersions, which is consistent with the theoretical prediction for bidispersed rod-like particles with different aspect ratios.[19] Potential applications include biologically compatible plasmonic composite nanomaterials for solar biofuel production and polarization sensitive plasmonic papers and fabrics.

In a first type of sample preparation, to obtain nematic-like ordering, we use CNCs right after the dialysis step of sample preparation described in the Experimental Section below. In the dilute regime with CNC concentrations below 3 wt%, both CNCs and GNRs are randomly oriented, as shown in **Figure 1**a. This is consistent with POM imaging that shows no birefringence in the isotropic phase (Figure 1b,c) as well as with polarization-independent extinction image and spectrum indicating a disordered dispersion of GNRs (Figure 1d,e). When the aqueous CNCs reach a critical concentration of about C_c~3 wt%, it forms an orientationally ordered birefringent dispersion schematically shown in Figure 1f. Its origin can be attributed to entropic steric interactions that minimize the so-called "excluded volume" and maximize the translational part of entropy (at the expense of orientational component of entropy), which is higher in a nematic phase as compared to a disordered isotropic phase and stabilizes the ground-state nematic phase above the C_c, which was first described theoretically by Onsager.[18] This behavior is strongly influenced by screened electrostatic interactions that arise due to charging of CNCs, which tend to increase the effective particle volume and thus reduce the C_c. Although most reports have seen only cholesteric phases with a helicoidal order that reduces Coulombic

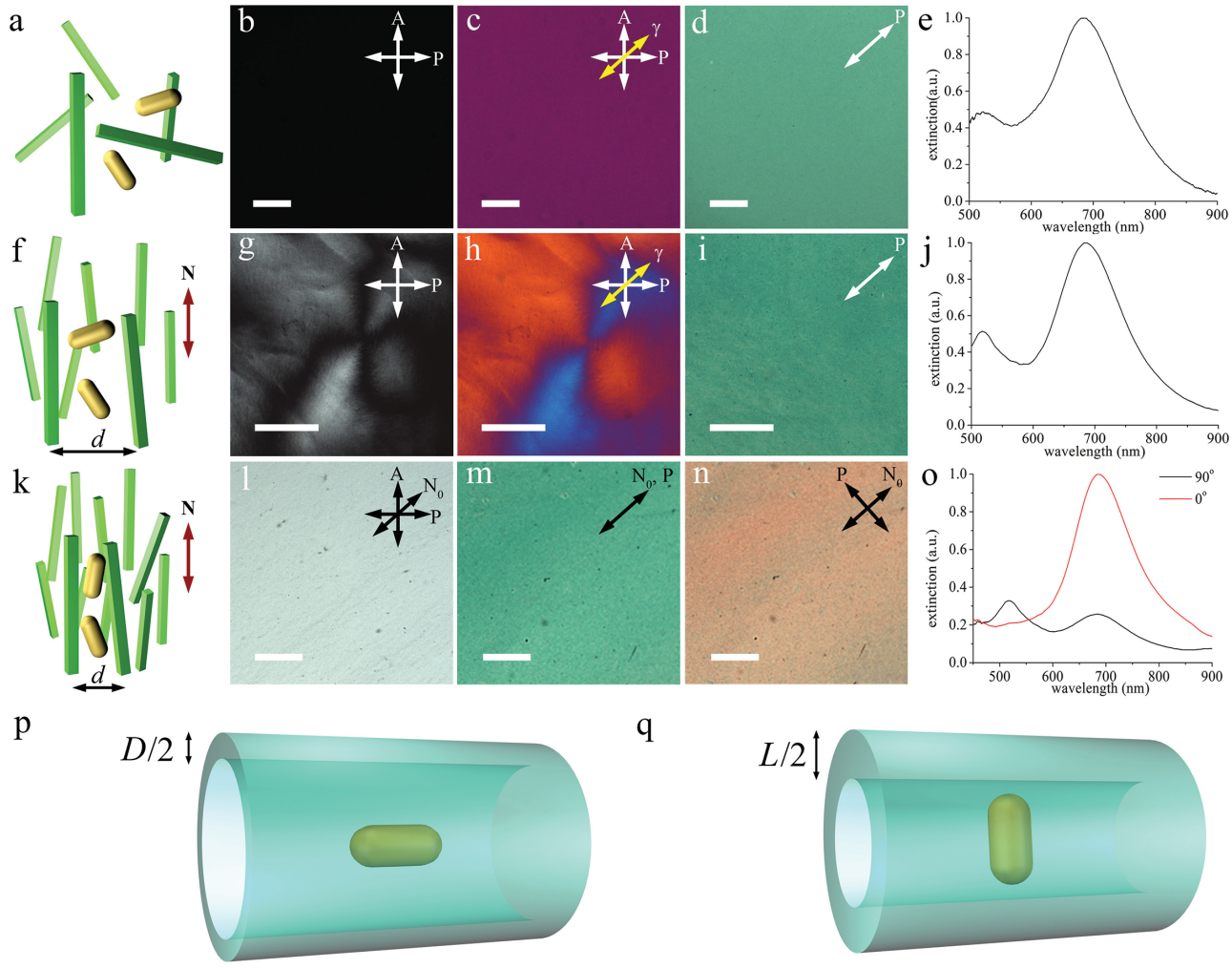

Figure 1. (a) Schematic of randomly dispersed GNRs (gold color) in a dilute CNC (green color) dispersion. POM images taken (b) without and (c) with a full-wavelength (530 nm) retardation plate with a slow axis (γ) marked by yellow arrow. (d) The transmission optical microscopy image and (e) polarization-independent extinction spectrum of GNR-CNC sample indicate the GNRs are unaligned. (f) Schematic of randomly dispersed GNRs in nematic-like CNCs with an average inter-CNC distance of d and local director **N**. POM images (g) without and (h) with the full-wavelength (530 nm) retardation plate having its slow axis marked with γ and a yellow arrow, showing an integer-strength defect line in a schlieren texture. (i) Transmission optical microscopy image and (j) polarized extinction spectrum show that the GNRs are unaligned. (k) Schematic of unidirectional aligned GNRs in nematic-like CNCs with an average distance of d and local director **N**. (l) POM textures of aligned nematic-like CNCs with a far-field director $\mathbf{N}_0$. Transmission optical microscopy image with (m) $\mathbf{P}||\mathbf{N}_0$ and (n) $\mathbf{P}\perp\mathbf{N}_0$. (o) The polarization-dependent extinction spectra of aligned GNRs and nematic-like CNC composites. Excluded volume of GNR in the CNC host dispersion with the average inter-CNC spacing setting a size of the effective confinement tube when GNR is (p) parallel and (q) orthogonal to **N**. All scale bars are 20 μm.

interactions between the rods, there are a few previous examples of nematic phase. Polydisperse CNCs with intrinsically twisted ribbon-like shapes and larger aspect ratios could be prepared to form nematic and cholesteric phases, depending on the ionic strength. The polydispersity and screened electrostatic interactions were previously shown tending to obscure the chiral morphology of nanocrystal dispersions, leading to nematic-like or long-pitch cholesteric order with roughly parallel orientations of rod-like CNCs of different aspect ratio.[20] Nematic-like ordering is also consistent with other literature reports. Hirai et al. found that bacterial cellulose concentrations that would normally produce biphasic cholesteric-isotropic systems produced a uniform untwisted phase after addition of salt.[21] Supramolecular polymerization has been suggested as a plausible mechanism for this system.[22] Although the complex interplay of molecular chirality, colloidal chirality, and electrostatic interactions is not completely understood, varying ionic strength, pH, and polydispersity can disrupt the helicoidal ordering. Using CNCs obtained immediately after dialysis with no further filtration, we have achieved a nematic-like ordering using cellulose dispersions derived from plants at a pH of ~1.0. Such a nematic-like specimen with rather polydisperse CNCs exhibited a schlieren texture with typical disclinations seen in POM micrographs obtained with full-wavelength (530 nm) retardation plate (Figure 1g,h). For CNCs with $n_{\|} = 1.595$ and $n_{\perp} = 1.534$,[23] the known positive refractive index anisotropy $\Delta n = n_{\|} - n_{\perp}$ along with the interference colors reveal that CNCs (and the nematic director **N** describing the local average

orientation of the nanocrystals) around the disclination orient radially. Although this texture clearly shows nematic-like ordering of CNCs, the distance between CNCs are still too large to prompt the alignment of relatively short GNRs, as the aspect ratio of CNCs is much larger than that of GNRs. Consequently, GNRs still exhibit random orientations, as evident from the polarization-independent extinction image and spectrum (Figure 1i,j).

With increasing the concentration of CNCs up to a second critical concentration, which for this type of samples was found to be about C_{c2} = 20 wt%, the excluded-volume effect due to GNRs in an aligned matrix of CNCs finally prompt the uniaxial alignment of GNRs along the local director **N** of the LC of CNCs (Figure 1k). At this concentration the CNCs are in a glassy state, in which the orientational ordering is frozen.[22,24] Under shear, these samples unidirectionally align to form nematic-like ordering with a uniform far field director $\mathbf{N}_0$ pointing along the shear direction (Figure 1l). These concentrated CNCs-GNRs composites show the characteristic polarization-dependent extinction colors (Figure 1m,n) and both longitudinal and transverse modes in the surface plasmon resonance spectra (Figure 1o). The polarized spectra of the nanocomposite reveal that the longitudinal SPR band is the strongest when the polarizer **P** is parallel to the long axes of GNRs and **N** while it is at minimum when **P** is perpendicular to the long axes and **N**. In contrast, the transverse SPR peak is the strongest when **P** is orthogonal to the long axes and **N** but becomes suppressed when **P** is rotated toward the long axes of nanorods and **N**. The polarization-dependent spectra shown in Figure 1o clearly demonstrate that GNRs align along $\mathbf{N}_0$ with a positive scalar order parameter *S*. We characterize the degree of ordering of GNRs based on extinction spectra by calculating the 3D order parameter as $S = (A_{\parallel} - A_{\perp})/(A_{\parallel} + 2A_{\perp})$, where $A_{\parallel}$ and $A_{\perp}$ are the extinction for $\mathbf{P}\|\mathbf{N}_0$ and $\mathbf{P}\perp\mathbf{N}_0$, respectively. The order parameter of GNRs can be calculated by using spectra shown in Figure 1o and is found to be 0.474 for this particular GNR-CNC co-dispersion. Thus, our findings show that co-dispersions of rod-like nanoparticles allow for aligning nanorods with relatively small aspect ratios that cannot spontaneously form ordered LC structures themselves.

The phase behavior of a pure CNCs aqueous solution can be controlled by varying sample preparation conditions[24] and can be understood by utilizing the Stroobants, Lekkerkerker and Odjik (SLO) theory,[25,26] which considers interactions caused by charged surfaces of CNCs, in addition to the excluded-volume effects and orientational entropy. The charged surfaces increase the effective diameter and introduce repulsive forces between rods. This allows the CNC's chiral structure to manifest itself in inter-particle interactions, resulting in twisted structures of the orientationally ordered mesophase. In our system, the dimensions of nanoparticles and the concentration of H^+ counterions of surface sulfate groups (pH ≈ 1.0) are sufficient to determine the critical concentration of different phases. The calculated concentrations of transitions from isotropic to biphasic region and then to the anisotropic phase are ~2.5 wt% and ~3.2 wt%, respectively, comparable to the experimental values.

The studied composites with well-dispersed and unidirectionally aligned GNRs are characterized by TPL and TEM imaging techniques. When the polarization of excitation light ($\mathbf{P}_{ex}$) is parallel to the long axis of GNR with the excitation wavelength in the vicinity of longitudinal SPR peak, the TPL signal is maximized. However, the TPL signal is at minimum when $\mathbf{P}_{ex}$ is perpendicular to the long axes of GNRs and the aligned far-field director $\mathbf{N}_0$, scaling as $\propto \cos^4\theta$, where θ is the angle between $\mathbf{P}_{ex}$ and $\mathbf{N}_0$. This polarization dependence is used to probe orientations of GNRs in CNCs aligned by shear force, supporting our finding that GNRs orient along $\mathbf{N}_0$ (**Figure 2**a,b). TEM images allow us to directly visualize the orientations and assembly of CNCs and GNRs. The emergence of local ordering in samples prepared from pure CNC dispersions can be seen in Figure 2c. GNRs added to such dispersion spontaneously follows the local spatially varying director of unaligned CNC dispersion (Figure 2d) and are unidirectionally aligned in a sheared GNR-CNC composites (Figure 2e).

We also studied CNC dispersions in the cholesteric phase, to provide a different type of ordering for GNRs. They were obtained with further purifying CNCs through additional centrifugation at 9000 rpm for 30 min and increasing pH to ~3. The twisted morphology of cellulose nanocrystals and the corresponding charging of their surfaces manifest themselves in the helicoidal ordering and in the formation of a cholesteric phase. When the suspension reaches the second critical concentration C_{c2}, GNRs start to follow the twisted local director of CNCs rotating around the helical axis χ (**Figure 3**a). These cholesteric samples of CNCs are examined by POM with full-wavelength (530 nm) retardation plate, displaying typical cholesteric LC "fingerprint" textures (Figure 3b,c). Three-dimentional patterns of GNR orientations in cholesteric CNC-GNR composites are probed by polarized TPL imaging, revealing that uniformly distributed GNRs in the planar cholesteric LC structures self-align with their long axes parallel to the helicoidal **N**. The observed structures have different helical axis orientations with respect to cell substrates. In the fingerprint textures with in-plane orientation of χ (Figure 3d,e), a TPL texture is a periodic pattern for $\mathbf{P}_{ex}\perp\chi$, while exhibiting a weak signal (dark) for $\mathbf{P}_{ex}\|\chi$. When imaging the vertical cross-section of the sample with χ perpendicular to the cell's surface, TPL textures taken for any combination of mutually orthogonal orientations of $\mathbf{P}_{ex}$ are found to be mutually complementary. A representive example of a mutually superimposed TPL textures obtained for two orthogonal polarizations is shown in Figure 3f. As the sample is excited by light with two orthogonal polarization $\mathbf{P}_{ex}\|\mathbf{x}$ (blue color) $\mathbf{P}_{ex}\|\mathbf{y}$ (yellow color), the TPL texture reveals the helicoidal configuration of GNRs mimicking that of the CNCs.

At CNC concentration of ~5 wt% corresponding to the biphasic regime, we observe cholesteric droplets surrounded by the isotropic phase (**Figure 4**a,b). In the isotropic phase, GNRs randomly orient while GNRs are aligned to form a helicoidal structure in cholesteric CNCs droplets (Figure 4c,d). A comparison of TPL images obtained for different polarizations of excitation light reveals that the concentration of GNRs in the isotropic surrounding is much higher than within the cholesteric drops (Figure 4c,d), which is a natural observation as the GNRs with the aspect ratio much smaller than that of CNCs are expected to separate out of the ordered dispersion of the nanocrystals above a certain "miscibility limit" while being relatively enriched within the orientationally disordered CNCs. This is in agreement with theoretical studies of bidispersed

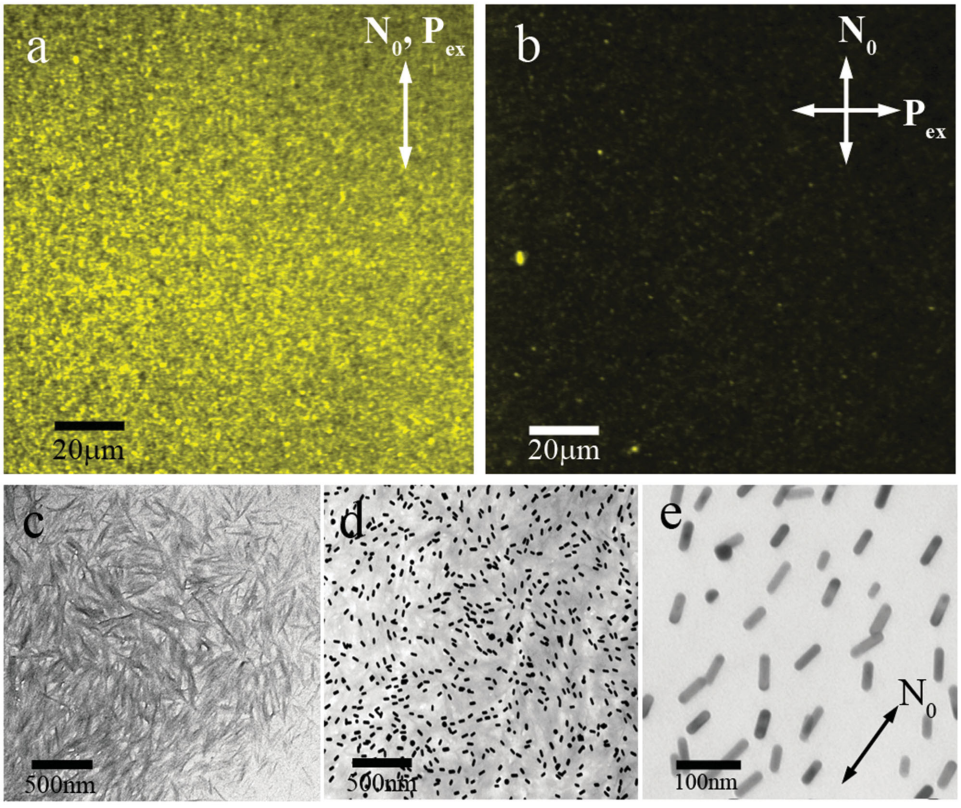

Figure 2. TPL images of unidirectionally aligned GNRs in nematic-like CNC with (a) $\mathbf{P}_{ex}||\mathbf{N}_0$ and (b) $\mathbf{P}_{ex}\perp\mathbf{N}_0$ show significantly stronger signal associated with rods parallel to the director. (c) TEM imaging of dropcast pure CNCs (d) and GNRs dispersed in CNCs show the GNRs align within a schlieren texture of the nematic-like director **N** with topological defects. (e) TEM image of unidirectionally aligned GNRs in a dispersion of CNCs with the far-field director marked by $\mathbf{N}_0$.

rods which predict a nematic phase rich in longer rods and an isotropic phase rich in shorter rods.[27–29] Since the GNRs have a smaller aspect ratio, the isotropic phase is enriched in GNRs, consistent with our experimental observations. The surface anchoring of the LC director at the cholesteric-isotropic interfaces is weak, so that the cholesteric structures remain undistorted at the interfaces (Figure 4). The orientation of helical axis in the drops is random and thermally fluctuates with time in smaller drops but it is found to be uniform within each droplet. These findings are consistent with an extension of the Onsager theory to bidispersed rod-like particles, which predicts LC-isotropic phase coexistence in mixtures of rods with two different aspect ratio,[28,29] similar to our system.

As the sample stays still for some time and solvent evaporates, thus further increasing the concentration of nanoparticles, the initially isolated cholesteric droplets grow in size. As the droplets merge, their helicoidal structures fuse forming a polydomain sample with the helical axes oriented along a different direction in each domain; the periodicity of fingerprint textures in each domain seen in POM images are found to be slightly different (**Figure 5**a,b), which is due to different oblique and in-plane orientation of the helical axes as well as sometimes slightly different intrinsic cholesteric pitch in domains emerging from different drops. In individual domains, CNCs as well as GNRs self-assemble into helicoidal structures, as revealed by POM and TPL images shown in Figure 5c-f, often becoming connected to a planar cholesteric texture in-between domains. These structured GNR-CNC composites have the potential to form free-standing bulk chiral materials with attactive SPR properties by drying the suspensions.[30]

To understand orientational ordering of GNRs within the CNC dispersion matrix, it is important to remember that the surfaces of our mPEG-functionalized GNRs are electrostatically neutral. Therefore, electrostatics plays no direct role in determining orientational ordering of GNRs within the CNC liquid crystalline matrix. Ordering of GNRs in this matrix at and above C_{c2} is driven by steric interactions of the GNRs with the host liquid crystalline CNC dispersion. The aspect ratio of GNRs (chosen to display the longitudinal SPR peak within the visible part of optical spectrum) is too small to allow for spontaneous nematic-like ordering in pure GNR dispersions, since the Onsager critical concentration cannot be reached (note that the original Onsager theory also cannot be applied to such rods with very small aspect ratios).[18] However, interaction of these small-aspect-ratio GNRs with the host dispersion of CNCs in both glassy nematic-like and cholesteric states can still lead to orientational ordering of GNRs to maximize their overall entropy. To qualitatively illustrate a possible physical mechanism behind this effect, one can assume that the GNRs are confined into an imaginary tube defined by neighboring CNCs (Figure 1p,q), with its diameter *d* equal to the inter-CNC spacing. Whilst parallel

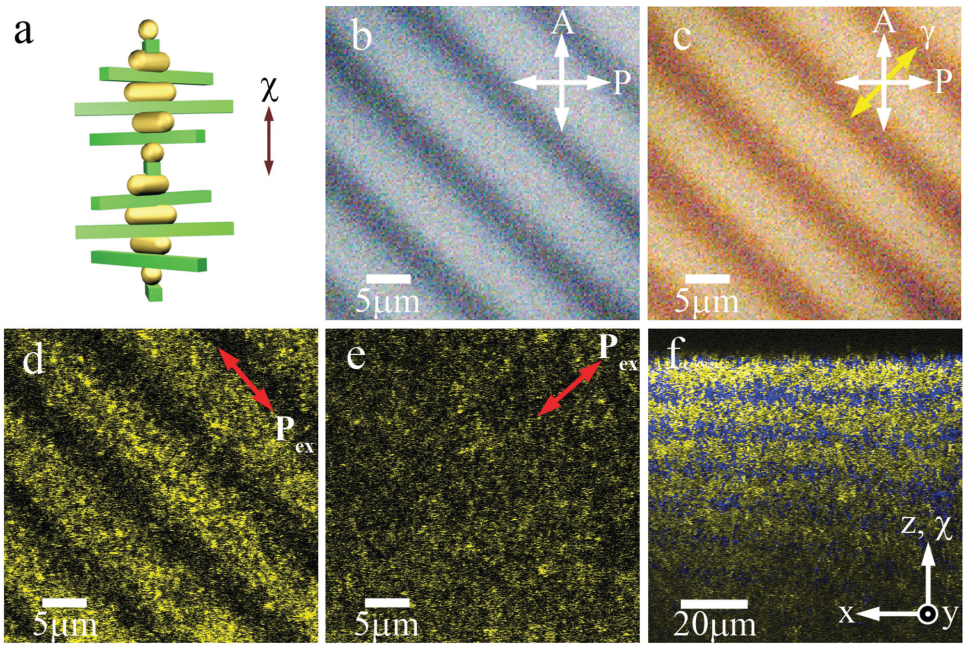

Figure 3. (a) Schematic of helicoidal assembly of GNRs in a cholesteric dispersion of CNCs. POM images of finger-print texture of GNR-CNC composites (b) without and (c) with a full-wavelength (530 nm) retardation plate with a slow axis (γ) marked by a yellow arrow. TPL images of the helicoidal assembly of GNRs in CNCs with (d) $\mathbf{P}_{ex}\perp\chi$ and (e) $\mathbf{P}_{ex}\|\chi$ (χ is parallel to the cell substrates). (f) Superimposed TPL images of the cross-section of GNR-CNC sample obtained for two orthogonal P_{ex} ($\chi\|\mathbf{z}$, thus perpendicular to the cell substrates), with the TPL signals corresponding to the two orthogonal polarizations shown in blue ($\mathbf{P}_{ex}\|\mathbf{x}$) and yellow ($\mathbf{P}_{ex}\|\mathbf{y}$) colors. The intensity of polarized TPL signals varies from minimal (black) to maximal (yellow and blue).

arrangements of CNCs along the tube lead to a decrease in orientational entropy, there is an increase in positional entropy determined by the volume within the tube accessible to centers of mass of GNRs (Figure 1p,q). The excluded volume of a GNR aligned along the tube's axis (and the director **N** of the CNC LC) is $V_{\|} = \pi(d-D)^2 l\,/\,4$ while the excluded volume of a GNR aligned perpendicular to **N** is $V_{\perp} = \pi(d-L)^2 l\,/\,4$, where l is the length of the tube, D and L are the diameter and length of a GNR. Since the perpendicular and oblique orientations of a GNR yield a larger excluded volume as compared to that of a GNR aligned along the tube and **N**, the decrease of inter-CNC distances with increasing their concentration leads to entropically favorable orientational ordering of GNRs within the CNC dispersion as the gain in translational entropy due to an increased accessible volume overcomes the corresponding orientational entropy reduction. Since the density of cellulose is 1.5 g/mL, 1.5 times that of water, the second critical concentration C_{c2} ~ 20 wt% in the nematic-like glassy state is equivalent to ~14 vol%, which corresponds to an estimate of $d \sim D$ at the critical concentration for alignment of GNRs. Orientational ordering of GNRs in biphasic cholesteric-isotropic samples occurs at lower global CNC concentrations ~5 wt% (Figure 4), at which the inter-rod distances are about L. This is only partially due to the fact that the concentrations of CNCs within isotropic and nematic-like domains of biphasic samples are different, with the ordered droplets being more concentrated in CNCs and thus capable of ordering GNRs within them. The observations suggests that the fluid nature of the cholesteric co-dispersion allows for reducing its C_{c2} as compared to that of the glassy nematic-like composites.

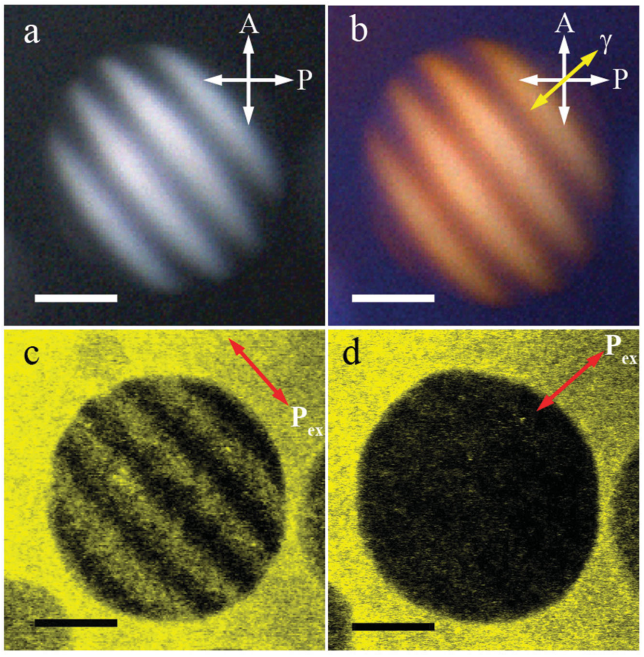

Figure 4. POM images of a droplet of cholesteric GNR-CNC composite surrounded by an isotropic phase obtained (a) without and (b) with a full-wavelength (530 nm) retardation plate with a slow axis (γ) marked by a yellow arrow. Corresponding TPL images obtained for (c) $\mathbf{P}_{ex}\perp\chi$ and (d) $\mathbf{P}_{ex}\|\chi$ (χ is parallel to the cell substrates). All scale bars are 30 μm.

In conclusion, we have demonstrated co-dispersion and oriented self-assembly of GNRs and CNCs into a variety of mesostructured composite materials with nematic-like, helicoidal cholesteric and LC-isotropic phase-coexistence structures. These

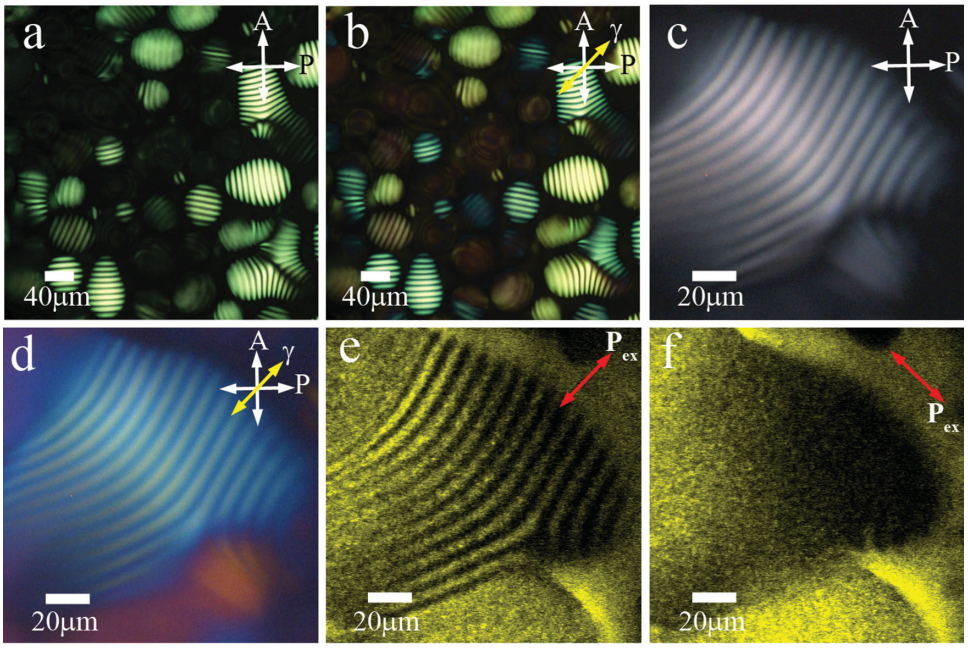

Figure 5. POM images of continuous domains of GNRs in cholesteric CNCs (a) without and (b) with a full-wavelength (530 nm) retardation plate with a slow axis (γ) marked by yellow arrow. POM images of enlarged continuous domains of GNRs in cholesteric CNC (c) without and (d) with a full-wavelength (530 nm) retardation plate with a slow axis marked by yellow arrow. Corresponding TPL images when (e) $\mathbf{P}_{ex} \perp \boldsymbol{\chi}$ and (f) $\mathbf{P}_{ex} \| \boldsymbol{\chi}$ ($\boldsymbol{\chi}$ is roughly parallel to the cell surface or tilted with respect to them).

composites promise scalable fabrication of structured materials with mesoscale orientationally ordered organization based on a renewable cellulose-based system. The phase behavior and structural organization are qualitatively consistent with predictions of extensions of the Onsager theory to charged and bidispersed colloidal suspension of rod-like particles with different aspect ratios. The unidirectional self-ordering of GNRs gives rise to the strong polarization sensitivity of SPR effects, potentially enabling scalable fabrication of plasmonic polarizers, smart windows, and various biologically compatible nanocomposites with SPR properties. The demonstrated self-assembly of organic-inorganic hybrid composite comprised of CNCs and gold nanoparticles can be potentially extended to other metal and semiconductor rod-like nanoparticles, such as quantum rods, magnetic nano-needles, and many other, thus providing means for scalable fabrication of mesostructured composites with pre-engineered optical, magnetic, electronic, and other properties. Although our goal in this work was to develop new material composites with orientationally ordered anisotropic plasmonic nanoparticles, our study also shows a great potential for using GNR-CNC mesomorphic systems to study stability and phase behavior of co-dispersions of charged and electrostatically neutral rod-like colloids with different aspect ratios. A promising recent direction of the biofuels research involves breaking down cellulose with enzymes to produce ethanol. Breaking down nanocrystalline cellulose can increase the yield.[31] The presense of co-dispersed ordered anisotropic plasmonic nanoparticles may additionally enhance the photoconversion processes that are also often a key part of biofuel production.[32]

Experimental Section

Synthesis, Functionalization of GNRs: GNRs with a mean width of 20 nm and a mean length of 50 nm were synthesized using a seed-mediated method.[33] Polymer grafting on the surface of GNRs was used to stabilize colloidal GNRs.[34] First, this GNR dispersion was centrifuged at 9000 rpm for 20 min twice and then re-suspended to 1 mL of deionized water to reduce the concentration of cetyltrimethylammonium bromide used for the growth and stabilization of nanorods. Then, 250 μL of an aqueous solution with 2 mM of 5 kDa thiol-terminated methoxy-poly(ethylene glycol) (mPEG-SH, JemKem Technology) was added into 5 mL of a 3.5 nM GNR dispersion. The mixture sat overnight and was purified via centrifugation to eliminate the excess mPEG-SH.

Synthesis of CNCs, Dispersion of GNRs in CNCs and Sample Preparation: Colloidal suspensions of CNCs were prepared by controlled sulfuric acid hydrolysis of cotton fibers, according to the method described by Revol and co-workers.[35] During this process, disordered or paracrystalline regions of cellulose are preferentially hydrolyzed, whereas crystalline regions, that have a higher resistance to acid, remain intact. 7g of cotton were added to 200g of 65 wt% sulfuric acid and stirred at 45 °C in a water bath for up to several hours until the cellulose had fully hydrolyzed. The mixture was sonicated occasionally, which was found to help degrade the amorphous cellulose regions. The suspensions of cellulose were then centrifuged at 9000 rpm for 10 min and re-dispersed in deionized water 6 times to remove the excess sulfuric acid. The resulting precipitate was placed into a dialysis tubing (MWCO 12000–14000, Thermo Fisher Scientific Inc.) in de-ionized water for three days until the water pH remained constant. The dimensions of CNCs are about 5–10 nm in cross-section and, on average, 100–300 nm in length.[14] These CNC dispersions were used to obtain nematic-like co-dispersions of CNCs and GNRs. Some of the suspensions were filtered through Millipore filter with 8 μm holes. The final aqueous suspensions of nanocrystals obtained using this method were approximately 2–3% in concentration by weight, and could be concentrated further by water evaporation at ambient conditions. Sulfuric acid reacts with the surface

hydroxyl groups of cellulose to yield charged surface sulfate esters that promote dispersion of the CNCs in water to yield negatively charged (surface) sulfate groups that promote a perfectly uniform dispersion of the whiskers in water via screened electrostatic repulsions. Finally, we dispersed mPEG-GNRs from an aqueous solution into the CNC-based LC and evaporated water from this dispersion to get the desired concentrations of GNR-CNC composites. The concentration of GNRs was varied within 0.1–0.5 wt%. The dilute pure CNCs and GNR-CNC aqueous dispersion samples were drop-dried on formvar coated copper grids for nanoscale characterization by TEM. In the drying process, CNCs can enter into a glassy state, which preserves qualitative features of orientational ordering of the constituent nanoparticles.[22] The aligned GNRs in CNCs co-dispersion sample for these experiments was prepared by additionally applying a shearing force with a pipet tip.

Optical Characterization: POM imaging of GNR-LC composites was performed using an optical microscope BX-51 (Olympus) equipped with 10×, 20×, and 50× dry objectives (all from Olympus) with numerical aperture NA = 0.3–0.9, a CCD camera (Spot 14.2 Color Mosaic, from Diagnostic Instruments, Inc.), crossed polarizers, and a 530 nm full-wavelength retardation plate. Extinction spectra were obtained using a spectrometer (USB2000-FLG, Ocean Optics) mounted on the same microscope. TPL imaging[36] was performed using linearly polarized excitation by an 800 nm light from a tunable Ti:Sapphire oscillator (140 fs, 80 MHz, Chameleon Ultra- II, Coherent) at an average power <1 mW in the sample plane. A 60× oil objective with NA = 1.42 was used for epi-detection of TPL within a 400–700 nm spectral range by a photomultiplier tube (H5784–20, Hamamatsu).

Acknowledgements

We thank Bohdan Senyuk, Taewoo Lee, and Yuan Zhang for discussions. This research was supported by the U.S. Department of Energy, Office of Basic Energy Sciences, Division of Materials Sciences and Engineering, under the Award ER46921, contract DE-SC0010305 with the University of Colorado.

Received: June 17, 2014
Revised: July 26, 2014
Published online: August 28, 2014

[1] G. M. Whitesides, B. Grzybowski, *Science* **2002**, *295*, 2418.
[2] O. E. Semonin, J. M. Luther, S. Choi, H.-Y. Chen, J. Gao, A. J. Nozik, M. C. Beard, *Science* **2011**, *334*, 1530.
[3] A. Mertelj, D. Lisjak, M. Drofenik, M. Čopič, *Nature* **2013**, *504*, 237.
[4] R. Elghanian, J. J. Storhoff, R. C. Mucic, R. L. Letsinger, C. A. Mirkin, *Science* **1997**, *277*, 1078.
[5] Q. Liu, B. Senyuk, J. Tang, T. Lee, J. Qian, S. He, I. I. Smalyukh, *Phys. Rev. Lett.* **2012**, *109*, 088301.
[6] T. A. Wood, J. S. Lintuvuori, A. B. Schofield, D. Marenduzzo, W. C. K. Poon, *Science* **2011**, *334*, 79.
[7] C. P. Lapointe, T. G. Mason, I. I. Smalyukh, *Science* **2009**, *326*, 1083.
[8] B. Senyuk, Q. Liu, S. He, R. D. Kamien, R. B. Kusner, T. C. Lubensky, I. I. Smalyukh, *Nature* **2013**, *493*, 200.
[9] P. Poulin, S. Holger, T. C. Lubensky, D. A. Weitz, *Science* **1997**, *275*, 1770.
[10] C. W. Hsu, B. Zhen, W. Qiu, O. Shapira, B. G. DeLacy, J. D. Joannopoulos, M. Soljačić, *Nat. Commun.* **2014**, *5*, 3152.
[11] R. Shenhar, T. B. Norsten, V. M. Rotello, *Adv. Mater.* **2005**, *17*, 657.
[12] C. Kuemin, L. Nowack, L. Bozano, N. D. Spencer, H. Wolf, *Adv. Funct. Mater.* **2012**, *22*, 702.
[13] Q. Liu, J. Tang, Y. Zhang, A. Martinez, S. Wang, S. He, T. J. White, I. I. Smalyukh, *Phys. Rev. E* **2014**, *89*, 052505.
[14] Q. Liu, Y. Ye, I. I. Smalyukh, *Nano Lett.* **2014**, *14*, 4071.
[15] Q. Liu, Y. Cui, D. Gardner, X. Li, S. He, I. I. Smalyukh, *Nano Lett.* **2010**, *10*, 1347.
[16] Y. Habibi, L. A. Lucia, O. J. Rojas, *Chem. Rev.* **2010**, *110*, 3479.
[17] K. E. Shopsowitz, H. Qi, W. Y. Hamad, M. J. MacLachlan, *Nature* **2010**, *468*, 422.
[18] L. Onsager, *Ann. N.Y. Acad. Sci.* **1949**, *51*, 627.
[19] A. S. Peranza, P. Sollich, *J. Chem. Phys.* **2002**, *117*, 5421.
[20] J. Araki, S. Kuga, *Langmuir* **2001**, *17*, 4493.
[21] A. Hirai, O. Inui, F. Horii, M. Tsuji, *Langmuir* **2009**, *25*, 497.
[22] J. P. Lagerwall, C. Schütz, M. Salajkova, J. Noh, J. H. Park, G. Scalia, L. Bergström, *NPG Asia Materials* **2014**, *6*, e80.
[23] E. D. Cranston, D. G. Gray, *Colloids Surf., A* **2008**, *325*, 44.
[24] W. J. Orts, L. Godbout, R. H. Marchessault, J.-F. Revol, *Macromolecules* **1998**, *31*, 5717.
[25] A. Stroobants, H. N. W. Lekkerkerker, T. Odijk, *Macromolecules* **1986**, *19*, 2232.
[26] X. M. Dong, T. Kimura, J. F. Revol, D. G. Gray, *Langmuir* **1996**, *12*, 2076.
[27] S. Elazzouzi-Hafraoui, J. L. Putaux, L. Heux, *J. Phys. Chem. B* **2009**, *113*, 11069.
[28] H. N. W. Lekkerkerker, Ph. Coulon, R. Van Der Haegen, R. Deblieck, *J. Phys. Chem.* **1984**, *80*, 3427.
[29] T. Odijk, H. N. W. Lekkerkerker, *J. Phys. Chem.* **1985**, *89*, 2090.
[30] J. H. Park, J. Noh, C. Schütz, G. Salazar-Alvarez, G. Scalia, L. Bergström, J. P. Lagerwall, *ChemPhysChem.* **2014**. *15*, 1477.
[31] W. Bai, J. Holbery, K. Li, *Cellulose* **2009**. *16*, 455.
[32] O. Jorquera, A. Kiperstok, E. A. Sales, M. Embirucu, M. L. Ghirardi, *Bioresour. Technol.* **2010**. *101*, 1406.
[33] J. Perez-Juste, L. M. Liz-Marzan, S. Carnie, D. Y. C. Chan, P. Mulvaney, *Adv. Funct. Mater.* **2004**, *14*, 571.
[34] G. von Maltzahn, A. Centrone, J.-H. Park, R. Ramanathan, M. J. Sailor, T. A. Hatton, S. N. Bhatia, *Adv. Mater.* **2009**, *21*, 3175.
[35] J.-F. Revol, H. Bradford, J. Giasson, R. H. Marchessault, D. G. Gray, *Int. J. Biol. Macromol.* **1992**, *14*, 170.
[36] M. G. Campbell, Q. Liu, A. Sanders, J. S. Evans, I. I. Smalyukh, *Materials* **2014**, *7*, 3021.